

DOI: 10.1002/cbic.201402541

# Detailed Structure–Function Correlations of *Bacillus subtilis* Acetolactate Synthase

Bettina Sommer,<sup>[a]</sup> Holger von Moeller,<sup>[b, c]</sup> Martina Haack,<sup>[a]</sup> Farah Qoura,<sup>[a]</sup>  
Clemens Langner,<sup>[b]</sup> Gleb Bourenkov,<sup>[d]</sup> Daniel Garbe,<sup>[a]</sup> Bernhard Loll,<sup>\*[b]</sup> and  
Thomas Brück<sup>\*[a]</sup>

Isobutanol is deemed to be a next-generation biofuel and a renewable platform chemical.<sup>[1]</sup> Non-natural biosynthetic pathways for isobutanol production have been implemented in cell-based and in vitro systems with *Bacillus subtilis* acetolactate synthase (AlsS) as key biocatalyst.<sup>[2–6]</sup> AlsS catalyzes the condensation of two pyruvate molecules to acetolactate with thiamine diphosphate and Mg<sup>2+</sup> as cofactors. AlsS also catalyzes the conversion of 2-ketoisovalerate into isobutyraldehyde,

the immediate precursor of isobutanol. Our phylogenetic analysis suggests that the ALS enzyme family forms a distinct subgroup of ThDP-dependent enzymes. To unravel catalytically relevant structure–function relationships, we solved the AlsS crystal structure at 2.3 Å in the presence of ThDP, Mg<sup>2+</sup> and in a transition state with a 2-lactyl moiety bound to ThDP. We supplemented our structural data by point mutations in the active site to identify catalytically important residues.

## Introduction

The imminent end of economically relevant petrochemical resources is driving the development of sustainable, biomanufacturing processes to generate biofuels and commodity platform chemicals.<sup>1</sup> Because of its hydrophobic properties and high caloric value isobutanol is noted as a novel renewable platform chemical and biofuel component. Both in vivo and in vitro isobutanol production processes have been reported.<sup>[1–5,7–9]</sup> The in vitro approach allows elimination of undesired metabolic side-reactions that reduce molecular efficiency. Cell-based isobutanol yields are currently just 2% (v/v) due to its toxic effects.<sup>[1,3]</sup> By contrast, in vitro isobutanol synthesis potentially offers a yield of 12% (v/v), and allows spontaneous phase separation and simplified product recovery procedures.<sup>[10]</sup> An essential biocatalyst of isobutanol biosynthesis is thiamine diphosphate (ThDP)-dependent acetolactate synthase (ALS; EC

2.2.1.6), which is involved in natural butane-2,3-dione biosynthesis.<sup>[11,12]</sup> ALS requires the cofactors ThDP and Mg<sup>2+</sup> in order to catalyze the decarboxylation of one molecule pyruvate and transfer of the resulting cofactor-bound hydroxyethyl group onto a second pyruvate molecule to make acetolactate (Figure 1 A). In a side reaction, the ALS of *Bacillus* (AlsS) catalyzes the decarboxylation of 2-ketoisovalerate (KIV) to isobutyraldehyde (Figure 1 A).<sup>[2]</sup> Pyruvate is an upstream intermediate in artificial isobutanol biosynthesis, and KIV is a key downstream intermediate.<sup>[6]</sup> Generally, the reaction with pyruvate is favored by wild-type AlsS, which shows poor conversion rates with KIV. These factors may contribute to the observation that, in cell-based isobutanol production attempts, wild-type AlsS did not show any 2-ketoacid decarboxylase (KDC) activity.<sup>[13]</sup> Because of its central role in synthetic isobutanol biosynthesis, enhancing the reactivity of AlsS towards KIV would potentially simplify the cell-free reaction cascade because a specific KDC enzyme activity could be eliminated.<sup>[6]</sup> Acetohydroxyacid synthase (AHAS) is a related enzyme of the family; it catalyzes the same reaction as ALS but in a different biochemical context. AHAS catalyzes the first step in the branched-chain amino acid biosynthesis pathways of valine, leucine, and isoleucine, and it requires flavin adenine dinucleotide (FAD).<sup>[14]</sup> However, FAD did not appear to be involved in catalysis in *Salmonella typhimurium*.<sup>[15]</sup> Prokaryotic AHASs and some eukaryotic AHASs have an additional regulatory subunit.<sup>[16]</sup> This implies a different reaction mechanism and structure–function relationship compared to ALS enzymes. Crystal structures are only available for the AHAS catalytic subunit from *Saccharomyces cerevisiae* (PDB ID: 1T9A)<sup>[17]</sup> and *Arabidopsis thaliana* (PDB ID: 1YHZ)

Our in-depth phylogenetic sequence analysis revealed that the ALS enzymes represent a distinct subclass of the ThDP-dependent enzyme family, of which the carboxylases are arche-


<sup>1</sup> Chemicals produced from renewables that can serve as starting points for the production of other functional compounds.

[a] Dr. B. Sommer, M. Haack, Dr. F. Qoura, Dr. D. Garbe, Prof. Dr. T. Brück  
Fachgebiet Industrielle Biokatalyse, Technische Universität München  
Lichtenbergstrasse 4, 85748 Garching (Germany)  
E-mail: brueck@tum.de

[b] Dr. H. von Moeller, C. Langner, Dr. B. Loll  
Institut für Chemie und Biochemie, Abteilung Strukturbiologie  
Freie Universität Berlin  
Takustrasse 6, 14195 Berlin (Germany)  
E-mail: loll@chemie.fu-berlin.de

[c] Dr. H. von Moeller  
moloX GmbH  
Takustrasse 6, 14195 Berlin (Germany)

[d] Dr. G. Bourenkov  
European Molecular Biology Laboratory  
Notkestrasse 85, 22603 Hamburg (Germany)

 Supporting information for this article is available on the WWW under <http://dx.doi.org/10.1002/cbic.201402541>.

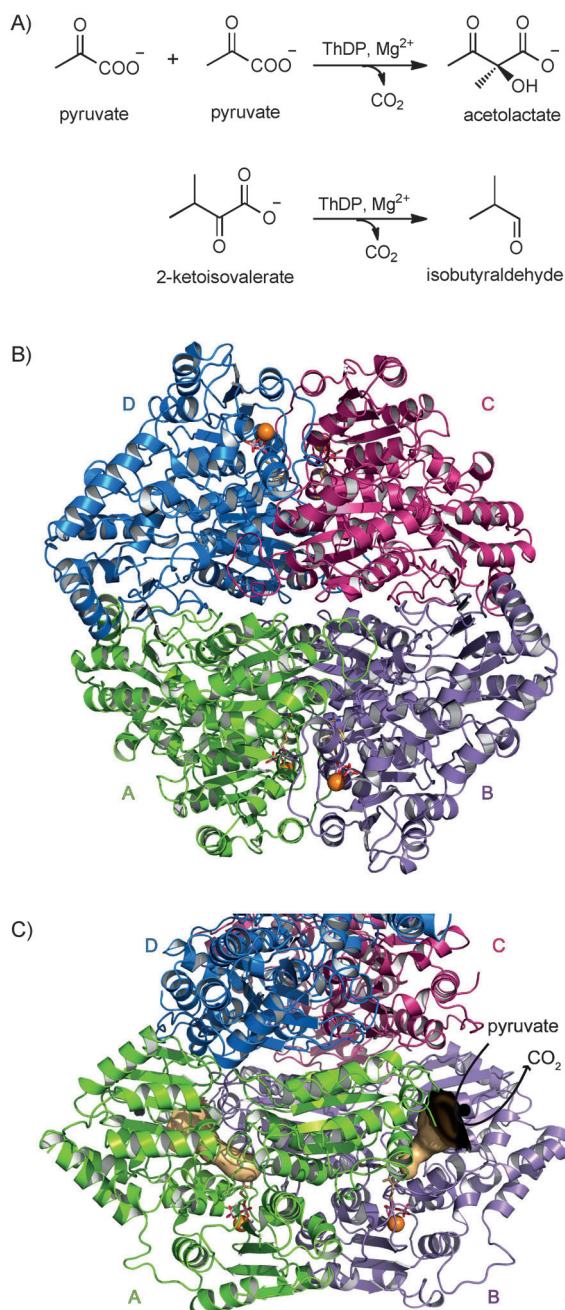


**Figure 1.** Reactions and structure of AlsS. A) The main reaction is the conversion of two molecules of pyruvate to acetolactate; the side reaction produces isobutyraldehyde. B) Overall structure of tetrameric AlsS<sup>wt</sup> (ribbon presentation) with Mg<sup>2+</sup> (orange spheres) and ThDP (stick representation). C) Solvent-accessible channels in monomers C and D are drawn in surface representation (beige). These point to the C2' atom of the ThDP cofactor and can be detected for all four monomers.

typical representatives. To date, structural information on ALS enzymes is limited to the structure of ALS from *Klebsiella pneumoniae* (AlsK, PDB IDs: 1OZF, 1OZG, 1OZH).<sup>[19]</sup> However structure-guided mutagenesis of AlsS could be a powerful tool to improve the catalytic properties of AlsS towards its native substrate pyruvate as well as KIV. In this study, we obtained valuable insights into the reaction mechanism of the ALS enzyme

family, by using a combined structural and biochemical approach. For the first time, we were able to elucidate the crystal structure of AlsS in the resting state and in a catalytically relevant transition state by X-ray crystallography. Structural data were used for targeted mutagenesis. Although the reaction mechanism and structure–function relationships of the archetypical ThDP-dependent enzyme family of carboxylases has been studied extensively, we demonstrate that the ALS subfamily differs significantly in structure and possibly in catalytic mechanism.<sup>[20]</sup> Certainly, our data suggest that the structure–function properties of AlsS not only differ from those of carboxylases but also show differences from the phylogenetically related AlsK.<sup>[19]</sup>

## Results and Discussion

### Phylogenetic analysis of ThDP-dependent enzymes

AlsS is an important biocatalyst in isobutanol biosynthesis, with dual catalytic activity: condensation of two pyruvate molecules to acetolactate, and conversion of KIV into isobutyraldehyde. This ability to catalyze both reactions is unique in the ALS family. This suggests that AlsS might have a different active-site architecture from that of other ThDP-dependent enzymes. We initially performed amino acid sequence alignments of diverse ThDP-dependent enzymes, and obtained information for a direct comparison of AlsS to the well-characterized ThDP-dependent decarboxylases (Figure S1 in the Supporting Information). For the latter family, a two-histidine motif (“HH-motif”), a fully conserved aspartate, as well as glutamate have been described.<sup>[21,22]</sup> These structural features are important for the correct orientation of the pyruvate molecule (Figure S1),<sup>[21,22]</sup> and establish a catalytic triad involved in the protonation of the enamine intermediate.<sup>[21–24]</sup> Our sequence alignment revealed that this motif is absent in ALS enzymes. Next, we performed a phylogenetic analysis of the ThDP-dependent enzymes. To our surprise, the enzymes clustered into three distinct sequence groups: acetolactate synthases, aceto-hydroxyacid synthases, and carboxylases (Figure S2). The alignment indicated that ALS active-site residues differ significantly from those of the well-studied carboxylase subgroup. It is also interesting to note that AlsS and AlsK are in different branches within the acetolactate synthase subgroup. Even though ALS and AHAS catalyze the same reaction, this likely reflects their different cofactors and domain structure: AHAS family enzymes have both catalytic and regulatory subunits. To shed light on the molecular architecture of AlsS, we set out to crystallize the protein and to determine its molecular architecture.

### Crystallization of AlsS

Wild-type AlsS (AlsS<sup>wt</sup>) and a C-terminal his-tagged variant (AlsS<sup>C-His</sup>) were overexpressed in *Escherichia coli* and purified to homogeneity for crystallization experiments. Prior to crystallization, the proteins were incubated with an excess of ThDP and Mg<sup>2+</sup>. Initially crystals of AlsS<sup>C-His</sup> were obtained in the tetragonal space group *P*4<sub>1</sub>2<sub>1</sub>2 (Table 1), and the crystal structure was

**Table 1.** Data collection and refinement statistics.

Data collection	AlsS <sup>C-His</sup> -ThDP	AlsS <sup>wt</sup> -ThDP	AlsS <sup>wt</sup> -LThDP
PDB ID	4RJI	4RJJ	4RJK
space group	<i>P</i> 4 <sub>1</sub> 2 <sub>1</sub>	<i>P</i> 2 <sub>1</sub> 2 <sub>1</sub>	<i>P</i> 2 <sub>1</sub> 2 <sub>1</sub>
wavelength [Å]	0.9184	0.9184	0.9763
unit cell <i>a</i> , <i>b</i> , <i>c</i> [Å]	141.7, 141.7, 239.0	111.3, 170.0, 340.0	111.5, 170.8, 342.6
$\alpha$ , $\beta$ , $\gamma$ [°]	90.0, 90.0, 90.0	90.0, 90.0, 90.0	90.0, 90.0, 90.0
resolution [Å] <sup>[a]</sup>	30.00–3.20 (3.39–3.20)	30.00–2.34 (2.48–2.34)	30.00–2.50 (2.56–2.50)
unique reflections	40 142 (6254)	26 8024 (41 131)	225 545 (16 544)
completeness <sup>[a]</sup>	99.5 (98.9)	98.4 (94.3)	99.8 (100.0)
$\langle I/\sigma(I) \rangle$ <sup>[a]</sup>	11.3 (2.5)	11.5 (3.0)	15.4 (3.2)
$R_{\text{meas}}$ <sup>[a,b]</sup>	0.206 (0.879)	0.108 (0.490)	0.133 (0.979)
$CC_{1/2}$ <sup>[a]</sup>	99.4 (81.5)	99.6 (80.6)	99.8 (86.4)
redundancy <sup>[a]</sup>	7.2 (7.1)	4.5 (4.1)	13.3 (14.2)
<b>Refinement</b>			
non-H atoms	16 994	36 644	35 466
$R_{\text{work}}$ <sup>[a,c]</sup>	0.187 (0.252)	0.172 (0.233)	0.166 (0.204)
$R_{\text{free}}$ <sup>[a,d]</sup>	0.253 (0.329)	0.217 (0.297)	0.217 (0.280)
no. of protein chains	4	8	8
<b>Average B-factor [Å<sup>2</sup>]</b>			
protein residues	2208/64.5	4416/24.2	4416/50.2
ThDP molecules	4/74.1	8/24.4	7/52.4
LThDP molecule	–	–	1/57.8
Mg <sup>2+</sup> cations	4/59.6	8/28.3	8/54.4
ligand molecules	1/84.4	33/37.7	47/63.3
water molecules	23/26.1	1955/24.9	837/45.3
<b>RMSD<sup>[e]</sup></b>			
bond length [Å]	0.005	0.009	0.010
bond angles [°]	0.890	1.177	1.220
<b>Ramachandran</b>			
outliers [%]	0.1	0.1	0.4
favoured [%]	97.8	98.0	97.0

[a] Values in parentheses refer to the highest-resolution shell. [b]  $R_{\text{meas}} = \sum_h [n/(n-1)]^{1/2} \sum_i |I_h - I_{h,i}| / \sum_h \sum_i I_{h,i}$ , where  $I_h$  is the mean intensity of symmetry-equivalent reflections and  $n$  is the redundancy. [c]  $R_{\text{work}} = \sum_h |F_o - F_c| / \sum_h F_o$  (working set, no  $\sigma$  cut-off applied). [d]  $R_{\text{free}}$  is the same as  $R_{\text{cyst}}$  but calculated on 5% of the data excluded from refinement. [e] RMSD from target geometries.

solved at medium resolution by molecular replacement with a poly-alanine model derived from *K. pneumoniae* ALS.<sup>[19]</sup> The asymmetric unit of AlsS<sup>C-His</sup> contains one homo-tetramer with bound cofactors ThDP and Mg<sup>2+</sup>. Attempts to improve the diffraction quality of these crystals failed. Therefore, we crystallized untagged AlsS<sup>wt</sup> and incubated it with ThDP and Mg<sup>2+</sup> under similar crystallization conditions. These crystals had a different crystal morphology compared to AlsS<sup>C-His</sup>, and diffracted to 2.34 Å resolution. Indexing of the diffraction data turned out to be very difficult, with various possibilities in monoclinic, orthorhombic, and tetragonal space groups. Finally, the diffraction patterns were indexed in the orthorhombic unit cell ( $a = 111.3$  Å,  $b = 170.0$  Å,  $c = 340.0$  Å). This indexing left out systematic weak reflections at positions  $h$ ,  $k + 1/2$ ,  $2L$ . The ratio of intensities of neglected satellite reflections to regular reflections was 0.033:1 on average in the resolution shell 30.0–2.5 Å.

Molecular replacement using the coordinates of one protomer of AlsS<sup>C-His</sup> derived from our medium-resolution data set as search model in space group *P*2<sub>1</sub>2<sub>1</sub> was successful. The unit cell contains eight ALS<sup>wt</sup> tetramers, four of which are formed

by the non-crystallographic symmetry (NCS) on a general symmetry position, and another four are at the intersections of the NCS axis and the crystallographic twofold axes. The structure of ALS<sup>wt</sup> was refined to  $R/R_{\text{free}}$  of 0.172/0.217 with excellent geometry (Table 1). The intensity modulation can be plausibly explained by the small deviations between the unit cell directions and the directions of twofold axes in mixed NCS crystallographic tetramers. Structure refinement using the data integrated in a double unit cell ( $a = 111.3$  Å,  $b = 340.0$  Å,  $c = 340.0$  Å; not shown) improved neither the refinement statistics nor the quality of the electron density maps. A detailed description of this crystal will be published elsewhere.

### AlsS architecture

The apparent biological unit of AlsS is a homo-tetramer formed by dimers of dimers (Figure 1 B) as reported previously for AlsK<sup>[19]</sup> and other ThDP-dependent enzymes such as pyruvate oxidase.<sup>[25]</sup> For a structural description, we shall focus on the highest-resolution structure of the complete tetramer in the asymmetric unit of the small unit cell of AlsS<sup>wt</sup>. Each monomer has 571 amino acids. The 13 N-terminal residues and five C-terminal residues could not be modeled due to the lack of interpretable electron density. The data suggest that these residues are highly flexible and do not form ordered structures. Each monomer is composed of three domains (Figure S3). The  $\alpha$ -domain (up to N181) is connected by a random coil to the central  $\beta$ -domain (P195 to A346). The C-terminal  $\gamma$ -domain (from H376) is connected to the central  $\beta$ -domain by an  $\alpha$ -helix and a random coil linker. Overall, the monomers of the tetramer are practically indistinguishable (RMSD < 0.3 Å). The ALS enzymes of *B. subtilis* and *K. pneumoniae* share 51% sequence identity. For 512 C $\alpha$  atoms, the structures show RMSD = 1.8 Å (Figure S4).

Yet there are major structural differences in ALS between *B. subtilis* and *K. pneumoniae*. A loop in the  $\alpha$ -domain of AlsS (K120 to S125) adopts a strikingly different conformation from that in AlsK (Figure S5). Interestingly, the loop is two amino acids longer in AlsS, and Q124 points to the active site. Notably, for AlsK the equivalent loop region (V118–Q120) is modeled in the “resting state”,<sup>[19]</sup> not in the catalytically relevant transition state. In contrast, for the AlsK structure, we could completely model the linker between the  $\alpha$ - and  $\beta$ -domain as a random coil (Figure S4).

AlsS and AlsK show additional differences in the linker region connecting the  $\alpha$ - and  $\beta$ -domains. These differences are particularly obvious between Q365 and D373 (AlsS) and in a loop region (R409 to T416) within the  $\gamma$ -domain (Figure S4). These differences result in distinct main-chain conformations, but these are distant from the active site and hence most likely have no functional implications. A comparison of the amino acid sequences of the less-conserved C termini of AlsS and AlsK reveals seven additional residues in AlsS. The 12 C-terminal resolved residues of AlsS (D556–K567) fold into a short  $\alpha$ -helix (Figure S4) that is not present in AlsK. This  $\alpha$ -helix packs onto the  $\beta$ -domain and is solvent exposed on the opposing site. This  $\alpha$ -helix is an extension of the structurally



conserved  $\alpha$ -helix that shields the ThDP and  $Mg^{2+}$  cofactors from the solvent.

### The active site

A substrate entrance channel extends 13 Å from the solvent-exposed surface to the active site (solvent-exposed diameter: 10–12 Å, narrowing towards the active site; Figure 1C). The wall of the channel comprises amino acid side chains of all three domains, as well as from both monomers of a functional dimer. The active site includes an  $Mg^{2+}$  ion and the ThDP cofactor (Figure 2A and Figure S6). The octahedral coordination of  $Mg^{2+}$  is established by two hydroxyl functions ( $\alpha$ - and  $\beta$ -phosphate of ThDP), the carboxylates of D451 and D478, the backbone carbonyl of T480, and one water molecule (Figure 2A).

In other ThDP-dependent enzymes,  $Mg^{2+}$  is coordinated by an asparagine at the equivalent position to D478.<sup>[26]</sup> Amino acid sequence analysis revealed that aspartate is strictly conserved in all known ALS sequences, and therefore seems to be characteristic for this subclass of ThDP-dependent enzyme. ThDP and  $Mg^{2+}$  were bound to all eight monomers, and hence we conclude that the structure represents the resting state of the enzyme. The four active sites of AlsS are at the two dimer interfaces (Figures 1B, C and 2). The  $Mg^{2+}$  cation is coordinated to residues of a single monomer, whereas the thiamine function of ThDP additionally interacts with residues of the adjacent monomer (Figure 2A). The ThDP is bound in a “V” conformation, maintained by the hydrophobic side chain of AlsS L426' from the neighboring subunit. The V conformation provides close proximity (3.1 Å) between the 4'-amino nitrogen and the C2' atom of ThDP. The pyrimidine function is stabilized by two hydrogen bonds. The first is to the carboxylate of E61', which is part of the adjacent monomer (Figure 2A). This interaction has been suggested to assist in the formation of the 4'-imino form of ThDP (Figure 2A).<sup>[27,28]</sup> The second hydrogen bond is established by the backbone carbonyl of Q424, thereby stabilizing the 4'-amino/imino group, which is then oriented for deprotonation of the adjacent C2' atom. This results in the reactive species (Figure 2A), which initiates the catalytic cycle. The phosphates of ThDP are stabilized by hydrogen bonds to protein side chains and backbone amides. Moreover, the N-terminal ends of three  $\alpha$ -helices (with their partial positive charge) point to the phosphates, thus conferring additional stabilization. Surprisingly there are no water molecules closer than 3.7 Å to the thiamine function of ThDP.

### A poly(ethylene glycol) (PEG) molecule in the vicinity of the active site

Interestingly, in two monomers of AlsS<sup>wt</sup> we observed elongated electron densities pointing to the C2' atom of the ThDP thiazole ring (Figure S7). We interpreted the electron density as PEG 200 molecules from the crystallization solution. It is somehow surprising to observe PEG molecules in an extended conformation, as they tend to adopt a horseshoe-like shape. The terminal hydroxyl of PEG 200 is 3.5 Å from the thiazole ring of

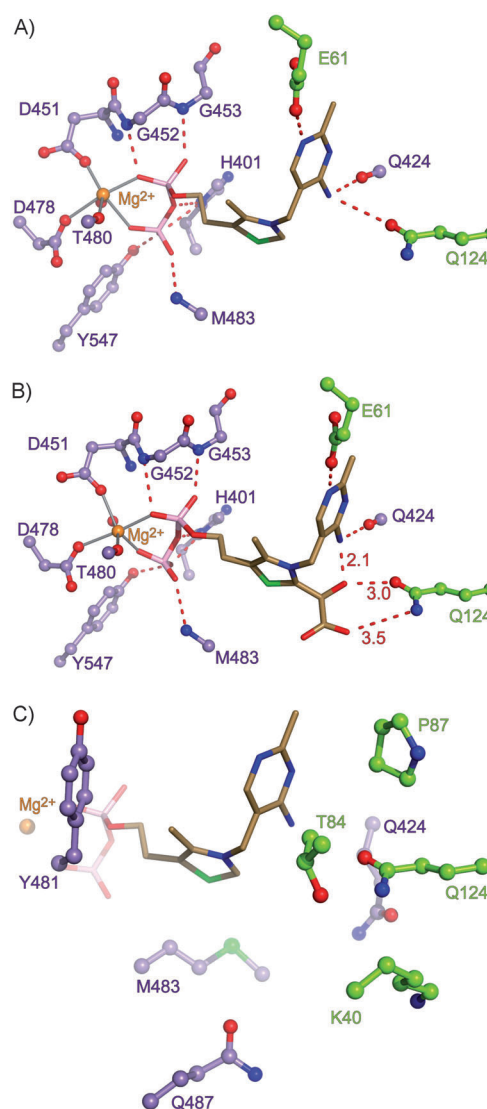


**Figure 2.** A) Active site of AlsS with bound ThDP and  $Mg^{2+}$ . Coordination of  $Mg^{2+}$  and interaction of ThDP with amino acids from two monomers lining the active site.  $Mg^{2+}$  and water molecules are drawn as spheres in orange and red, respectively. Grey lines indicate the coordination sphere of  $Mg^{2+}$ . Hydrogen bonds are drawn as dashed red lines (distance cut off 3.5 Å). B) As above but with bound LThDP and  $Mg^{2+}$ . C) Amino acid residues at the active site that have been subjected to site-directed mutagenesis.

ThDP. There are no direct interactions to the protein backbone, but rather indirect contacts (via water molecules). The hydroxy group of T84 interacts via a water molecule with the terminal hydroxy group of the PEG molecule (3.2 Å). Given the proximity of PEG to ThDP and the side chain of T84, we investigated the potential importance of this residue for correct positioning of the second pyruvate molecule.

### Catalytic aspects of structural features

To obtain structural information relevant to the catalytic cycle of AlsS, we soaked AlsS<sup>wt</sup> crystals in solutions of pyruvate. We observed the evolution of gas bubbles at the surface of the

crystals. Most likely the gas bubbles were CO<sub>2</sub> from the decarboxylation step of the reaction cycle. We determined the crystal structure of pyruvate-soaked crystals to 2.50 Å and refined them to  $R/R_{\text{free}}$  of 0.166/0.217. In simulated annealing with  $2F_o - F_c$  and  $F_o - F_c$  electron-density maps, we observed additional electron density in close vicinity to the C2' atom of ThDP. The shape and level of the electron density differed between the monomers. However, for one monomer it was directly connected to the C2' atom of the thiazolium ring. The connecting electron density perpendicular to the thiazolium ring of ThDP was unambiguously identified as a 2-lactyl moiety bound to ThDP (LThDP) with an sp<sup>3</sup>-hybridized C $\alpha$  atom (Figure 2B). Our structure of AlsS<sup>wt</sup> with LThDP represents a catalytically relevant transition state. This is the first time that the structure of any catalytically relevant reaction intermediate has been reported for any member of the ALS enzyme family, although it has been reported for other ThDP-depending enzymes.<sup>[21,24,29]</sup> Examination of AlsS<sup>wt</sup> with bound LThDP indicated that the 2-lactyl moiety bound to ThDP is stabilized by several interactions to protein side chains and to the core ThDP moiety. Interestingly, Q124 (pointing to the active site cavity) forms a bifurcated hydrogen bond to the carboxylate and hydroxyl of LThDP (Figure 2B). Furthermore, the hydroxyl of LThDP forms a short intermolecular hydrogen bond to the 4'-amino group of the pyrimidine (Figure 2B). The pyruvate-derived methyl points towards M483. This overall arrangement is very similar to that of pyruvate oxidase.<sup>[29]</sup> Kinetic studies of other ThDP-dependent enzymes revealed that the 4'-amino group of the pyrimidine moiety acts as the proton donor for pyruvate.<sup>[30]</sup> The short hydrogen bond observed in our structure is consistent with this function of the 4'-amino group. Wille et al. proposed that a distortion of the aromatic thiazolium ring might assist in the decarboxylation reaction.<sup>[29]</sup> Because of the limited resolution we could not detect this ring distortion in our crystal structure. Notably, no major conformational rearrangements occurred to amino acid side chains in the active site or to the bound cofactor upon binding of pyruvate to ThDP. We could not detect any pyruvate molecule in close proximity to the active site or in the channel. Instead, two molecules of pyruvate were identified on the protein surface.

### Biochemical characterization of AlsS<sup>C-His</sup>

In baseline measurements of ALS variants, we verified that AlsS<sup>wt</sup> and AlsS<sup>C-His</sup> have identical activities. AlsS is a key enzyme in a recently published cell-free isobutanol biosynthesis pathway.<sup>[6]</sup> To assess the performance of these AlsS variants in isobutanol production, the stability and activity of each enzyme in the presence of process-relevant alcohols (isobutanol, butanol, and ethanol) were measured. To determine the catalytic activity of AlsS towards pyruvate we applied a previously reported coupled assay with lactate dehydrogenase (LDH).<sup>[31]</sup> In brief, the reactions take place in two steps. In the first step AlsS converts pyruvate to acetolactate. At intervals, samples are taken and immediately added to the second step mixture, in which the remaining pyruvate is converted to lac-

tate. The catalytic activity of LDH can be measured photometrically (340 nm) by following NADH depletion. Hence, the amount of consumed pyruvate by AlsS can be calculated. The assay conditions for both AlsS and LDH are flexible and can be readily adapted; however, the LDH assay temperature must be maintained at 25 °C. We performed a detailed characterization of AlsS<sup>C-His</sup> to determine its temperature optimum, its half-life at 50 °C, its solvent stability at pH 7.0, and its pH tolerance at 50 °C. Incubation at 50 °C and pH 7.0 was chosen for the subsequent assays, as these conditions were well tolerated by all enzyme components of the cell-free isobutanol biosynthesis pathway.<sup>[6]</sup>

### Activity of AlsS variants towards the alternative substrate KIV

The activities of AlsS towards both pyruvate and KIV are relevant for reducing the complexity of cell-free isobutanol production (Figure 1 A). Therefore, increasing the activity towards both was an objective of our study. Thus, information on amino acid residues critical for the decarboxylation step with KIV is required. Atsumi et al. reported 5.5 U mg<sup>-1</sup> for the KDC activity of AlsS<sup>wt</sup>.<sup>[2]</sup> In this study we could not reproduce these results under equivalent experimental conditions (37–40 °C); we observed 1000-fold lower activity (maximum 53 mU mg<sup>-1</sup>). Subsequently, we prepared a set of mutants that are described in detail below. The lower  $K_M$  of AlsS<sup>Q487S</sup> (154 ± 21 mM) compared to that of AlsS<sup>C-His</sup> (300 ± 35 mM) did not result in a higher activity towards KIV (Table 2). However AlsS<sup>K40I</sup> showed a slightly improved activity (59 mU mg<sup>-1</sup>) towards KIV. AlsS catalyses the conversion of pyruvate to acetolactate as well as the decarboxylation of KIV to isobutyraldehyde, albeit at a much lower rate (Figure 1 A). As both reactions are required for the designed isobutanol synthesis, increasing the AlsS activity towards KIV could significantly lower the overall reaction complexity. To determine KIV specific activity, a coupled assay of AlsS with alcohol dehydrogenase (ADH) was applied. In this assay, KIV is converted to isobutyraldehyde by AlsS, then isobutyraldehyde is converted to isobutanol by ADH. This reaction can be measured photometrically at 340 nm because ADH

**Table 2.** Activities and half-lives of all AlsS<sup>C-His</sup> variants at 50 °C with pyruvate as substrate. Activities of all AlsS<sup>C-His</sup> variants towards KIV are also reported.

Protein	A [U mg <sup>-1</sup> ] at 50 °C	$t_{1/2}$ [h] at 50 °C	A <sub>KIV</sub> [U mg <sup>-1</sup> ] at 40 °C
AlsS <sup>HisC</sup>	24 ± 4.00	81	0.053 ± 0.0020
AlsS <sup>K40H</sup>	4 ± 0.20	44	0.045 ± 0.0080
AlsS <sup>K40I</sup>	3 ± 0.10	89	0.059 ± 0.0020
AlsS <sup>K40Y</sup>	7 ± 0.60	110	0.031 ± 0.0020
AlsS <sup>T84V</sup>	1 ± 0.08	2.5	0.021 ± 0.0020
AlsS <sup>P87A</sup>	18 ± 2.54	33	0.020 ± 0.0030
AlsS <sup>Q124S</sup>	6 ± 0.50	42	0.014 ± 0.0003
AlsS <sup>Q424S</sup>	27 ± 5.00	104	0.028 ± 0.0020
AlsS <sup>Q424S/Q487S</sup>	2 ± 2.00	94	0.016 ± 0.0010
AlsS <sup>Y481A</sup>	1 ± 0.06	19	0.004 ± 0.0010
AlsS <sup>M483N</sup>	–	–	0.009 ± 0.0020
AlsS <sup>Q487S</sup>	35 ± 2.00	22	0.046 ± 0.0030

concomitantly oxidizes NADH. Because of the moderate thermostability of horse liver ADH used in our assay, all KIV assays were carried out at 40 °C. Under these conditions AlsS<sup>C-His</sup> showed 53 mU mg<sup>-1</sup>.<sup>[32]</sup>

### Determination of pH and temperature optima for AlsS<sup>C-His</sup>

At pH 4.0 (and 50 °C) no activity was observed, but an activity profile was obtained over pH 5.0–6.0, with a plateau at pH 7.0–8.0; the activity reduced over pH 9.0–11.0 and at pH 11 no activity was detected (Figure 3 A). Thus, AlsS<sup>C-His</sup> showed excellent

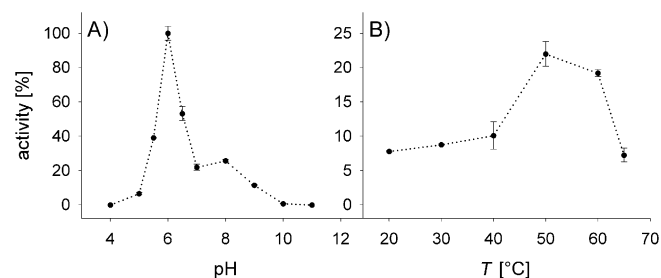


**Figure 3.** Determination of pH stability and temperature optimum of AlsS<sup>C-His</sup>. A) 50 mM sodium acetate (pH 4.0 and 5.5), 50 mM sodium phosphate (pH 6.0 to 6.5), 50 mM Tris (pH 7.0–9.0), or 50 mM CAPS (pH 10 and 11); all measurements at 50 °C. B) Enzyme assays for temperature optimum determination were performed from 20 to 65 °C at pH 7.0. Data are mean of three replicates; 100% activity is the highest measured activity in the experiment.

activity over pH 5.5–6.5 with an optimum at pH 6.0. The activity at pH 6.0 was six times higher than at pH 7.0. In the context of cell-free isobutanol biosynthesis, the pH optimum at pH 6.0 is a prerequisite for subsequent decarboxylation of acetolactate by action of an acetolactate decarboxylase, or by a low pH in the cell-based 2,3-butanediol production pathway.<sup>[11]</sup> This AlsS<sup>C-His</sup> pH profile is consistent with data observed for other members of ALS enzyme family.<sup>[33,34]</sup>

At the optimum temperature (50 °C) the activity of AlsS<sup>C-His</sup> (24 ± 4 U mg<sup>-1</sup> at pH 7.0) was almost three times higher than at 20, 30, and 65 °C (Figure 3B). At 50 °C and pH 7.0, we measured an AlsS<sup>C-His</sup> half-life of 81 h, and it was 16 h at 60 °C. The stability at 60 °C is rather surprising, as *B. subtilis* is a mesophilic bacterium; the optimal temperature for ALS derived from the mesophilic bacterium *Enterococcus faecalis* (AlsE) has been reported to be 37 °C.<sup>[32]</sup> In contrast, to AlsS, AlsE shows no temperature stability at temperatures above 40 °C.<sup>[32]</sup> The extended temperature stability observed for AlsS might be due to its specific architecture.

### Determination of AlsS<sup>C-His</sup> solvent tolerance

The production of solvents like isobutanol implicitly requires the enzyme to tolerate the end-products. In cell-based systems, 1–2% (v/v) isobutanol induced toxic effects in the host.<sup>[6]</sup> Therefore, in our assay, AlsS<sup>C-His</sup> activity was determined at 0–6% (v/v) isobutanol and *n*-butanol, and 0–20% (v/v) ethanol (Figure 4 A). The enzyme retained 50% activity in the presence

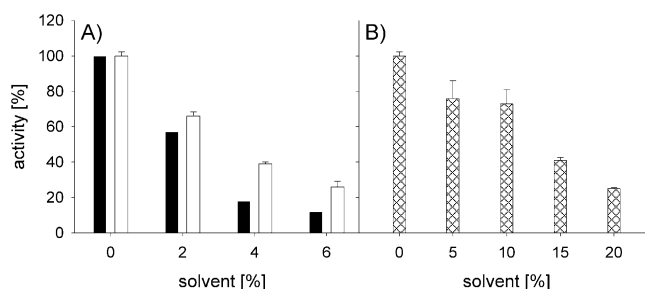


**Figure 4.** Solvent tolerance of AlsS<sup>C-His</sup> at 50 °C and pH 7.0 for A) 0–6% (v/v) *n*-butanol (■) and isobutanol (□) and B) 0–20% (v/v) ethanol.

of 3% (v/v) isobutanol and *n*-butanol, and of up to ~13% (v/v) ethanol (Figure 4B).

To our knowledge this is the first account of isobutanol tolerance by any member of the ALS family. Our ethanol tolerance results for AlsS mirror those obtained for AlsE (~50% activity up to 15% (v/v)).<sup>[35]</sup>

### Structure-guided mutagenesis strategy to generate AlsS variants

An examination of the AlsS active-site structure indicates that only a few residues are in proximity of the bound ThDP cofactor or the reaction intermediate LThDP (Figure S8). Interestingly, the AlsS residues are substantially different from their equivalents in ThDP-dependent enzymes involved in the decarboxylation of  $\alpha$ -ketoacids; these have been studied in great detail.<sup>[24]</sup> The degree of conservation within ALS enzymes suggests that ALS enzymes constitute a distinct subclass of ThDP-dependent enzymes. Based on structural assessment we selected eight amino acid residues in the vicinity of the ThDP binding site, for targeted single- or double-mutation replacement (Figure 2C). Even though AlsS and AlsK share only 55% amino acid identity, all our mutated amino acids are conserved in AlsK. A primary target was Q124, which is within hydrogen-bonding distance of LThDP (Figure 2A and B). Interestingly, the side chain of Q424 points directly towards LThDP; this indicates an involvement in the positioning the second pyruvate moiety in the active site to facilitate the second condensation reaction that yields acetolactate. Other mutagenesis targets were M483 and Q487 because their side chains are on an  $\alpha$ -helix and separated by one  $\alpha$ -helical turn (Figure S8). Hence, both side chains point in the same direction, towards the cofactor. Another target was Y481, on the opposite site of the catalytically active C2' atom of ThDP. Therefore Y481 might be important for the accurate positioning of ThDP. Additionally, we selected K40, whose homologue in AlsK (K36) is thought to be involved in catalysis.<sup>[19]</sup> Amino acid residue replacement was achieved by site-specific mutagenesis. All AlsS variants were expressed with a C-terminal His<sub>6</sub>-tag and characterized for activity towards pyruvate at 50 °C and pH 7.0 (HEPES buffer), as this pH is the most compatible with the enzyme systems involved in our artificial, cell-free isobutanol cascade.<sup>[6]</sup>

## Conclusion

The substrate promiscuity of AlsS towards pyruvate and KIV makes it potentially ideal for a minimized enzyme reaction cascade. Initially, the activities of wild-type AlsS towards pyruvate and KIV were determined: the activity towards KIV ( $53 \text{ mU mg}^{-1}$ ) was a side reaction compared to the  $2400 \text{ mU mg}^{-1}$  measured for pyruvate. AlsS<sup>wt</sup> had a pH optimum at pH 6.0 and exhibited maximum activity at 50 °C. In addition, AlsS<sup>wt</sup> tolerated higher product concentrations (50% activity in the presence of 3% (v/v) isobutanol/*n*-butanol, or 13% (v/v) ethanol) than did microbial hosts.

We also obtained detailed structural information on AlsS and its catalytic intermediate. The crystal structures allowed us to identify catalytically important residues in the active site of AlsS. Based on this information we generated AlsS variants, which were characterized for activity towards pyruvate and KIV (Table 2).

As proposed for other ThDP-dependent enzymes,<sup>[36]</sup> the catalytic cycle is initiated by proton abstraction from the 1',4'-iminopyrimidine tautomer of the ThDP cofactor by the conserved aspartate (E61 in AlsS) to yield the reactive ThDP. For other ThDP-dependent enzymes the HH-motif, a conserved aspartate, and a glutamate have been described as important for the correct positioning of the pyruvate molecule (Figure S1).<sup>[21,22]</sup> It had been proposed that the signature motif forms a catalytic triad involved in the protonation of the enamine intermediate of *Zymomonas mobilis* pyruvate decarboxylase (Figure 5 and Figure S1).<sup>[21,23,24]</sup>

The active site residues are different in AlsS compared to other ThDP-dependent enzymes. AlsS has A39 at the equivalent position of the conserved aspartate (E27) of *Z. mobilis* decarboxylase (Figure 5); this is conserved across other ALS enzymes (Figure S1). The HH-motif is not present in ALS enzymes. In place of the second histidine, AlsS has Q124, again conserved within the ALS family (Figure S1), and the flanking regions of the HH-motif in ALS enzymes (Figure 5) are longer in other ThDP-dependent enzymes. A loop region in our AlsS structure (L92 to S125) differs from that in AlsK and allows Q124 to approach the active site (Figure S5). In the crystal

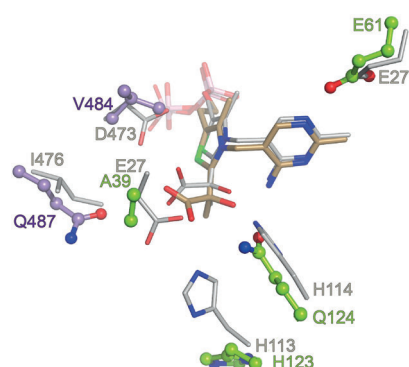


**Figure 5.** Superposition of active site residues of AlsS (green and violet) and pyruvate decarboxylase (PDZ, gray) of *Z. mobilis* (PDB ID: 3OE1),<sup>[21]</sup> with bound LThDP cofactor (AlsS: sand; PDZ: gray). The HH-motif of *Z. mobilis* PDZ is formed by H113 and H114.

structure of AlsS bound to LThDP, the 2-lactyl moiety is stabilized by the side chain of Q124 (Figure 2B). The importance of this for catalysis was confirmed by the drastically decreased activity of AlsS<sup>Q124S</sup> (Figure 1C and Table 2).

In the AlsK reaction model, K36 has been proposed to be important for recognition and correct positioning of the second pyruvate molecule.<sup>[19]</sup> The corresponding residue in AlsS (K40) has an identical side-chain orientation. In other ThDP-dependent carboxylases, tyrosine or phenylalanine are frequently at this sequence position. Replacement of K40 (Figure 1C) by the hydrophobic amino acid isoleucine (AlsS<sup>K40I</sup>), basic histidine (AlsS<sup>K40H</sup>), or tyrosine (AlsS<sup>K40Y</sup>) greatly reduced activity (Table 2).

The proximity of a PEG 200 molecule to ThDP and the hydroxyl function of T84 inspired variant AlsS<sup>T84V</sup> in order to investigate whether this residue is involved in substrate positioning. AlsS<sup>T84V</sup> cannot establish a hydrogen bond to PEG 200. In our enzymatic assays, the enzymatic activity was almost completely abolished, thus highlighting the importance of this residue.

AlsS<sup>Y481A</sup> showed almost complete loss of activity (Table 2). This residue not only lines the active site, but, with its hydroxyl group, it is hydrogen bonded to the carbonyl backbone of A58, thereby clamping the  $\beta$ - and  $\alpha$ -domains to each other. Disruption of this interaction does not only locally affect the cofactor binding site but most likely the overall stability of AlsS. The pyrimidine function of ThDP faces P87 at the N terminus of an  $\alpha$ -helix (Figure 1C). Mutation to alanine reduced the activity by about one third (Table 2), likely caused by reorientation of ThDP. Q424 and Q487 are on opposing sides of the tunnel leading to the active site. The side chains of these residues are oriented towards the C2' of ThDP or the 2-lactyl moiety of LThDP, and are potentially important for recognition and positioning of the second incoming pyruvate molecule. The backbone carbonyl of Q424 is hydrogen bonded to ThDP (Figure 2A and B), but there is no direct interaction between Q487 and ThDP. The side chains of Q424 and Q487 are 4.6 and 3.8 Å from the carboxylate function of LThDP. Therefore both amino acid residues were subjected to mutagenesis. Surprisingly, we detected increased activities towards pyruvate when Q424 or Q487 was mutated to serine (Table 2), although the double mutant AlsS<sup>Q424S/Q487S</sup> had only residual activity (Table 2), thus supporting the hypothesis that at least one residue is important for positioning the second pyruvate molecule.

Our structural findings are in agreement with our phylogenetic analysis of ThDP-dependent enzymes (Figure S2). The AlsS enzyme clusters in a distinct subgroup, with different amino acids at its active site from those in other ThDP-dependent enzymes. Our data show for the first time that the ALS subfamily of ThDP-dependent enzymes differ in both structure and function compared to the archetypical carboxylases and the AHAS enzyme family. Whether or not these structure–function differences have a significant impact on the general catalytic mechanism of ThDP-dependent enzymes, models for which have been developed based on the carboxylase, remains to be elucidated.



## Experimental Section

**Reagents and bacterial strains:** Restriction enzymes, T4 ligase, desoxynucleotides, phusion polymerase, DNA and protein-standards were purchased from Thermo Scientific; Klenow fragment and T4 kinase were from New England Biolabs. DNA sequencing and oligonucleotides synthesis were performed by Eurofins MWG Operon (Ebersberg, Germany). The acetolactate synthase gene from *B. subtilis* was synthesized by Genearth (Life Technology, Regensburg, Germany) with optimized *Escherichia coli* codon usage. Horse liver ADH was obtained from evocalat (Düsseldorf, Germany). Porcine heart LDH was from Serva (Heidelberg, Germany). 3-Methyl-2-oxobutanoic acid, thiamine diphosphate, and isobutyraldehyde were purchased from Sigma–Aldrich. Other chemicals were purchased from Carl Roth or from AppliChem (Darmstadt, Germany). pET28a was purchased from Merck Millipore. *E. coli* HMS174(DE3) was purchased from Merck Millipore, *E. coli* XL1-Blue was from Stratagene (Agilent Technologies).

**Cloning:** *B. subtilis alsS* was cloned into the vectors pCBRHisC (AlS<sup>C-His</sup>) and pCBRHisNo (AlS<sup>wt</sup>) at BfuI and BsaI restriction sites.<sup>[6]</sup> The exchanges were done using the megaprimer PCR method (Table S1).<sup>[37]</sup> PCR products were digested with XhoI and NcoI and ligated into pET28a.

**Protein expression and purification for crystallization:** Plasmids coding for AlS<sup>wt</sup> or AlS<sup>C-His</sup> were transformed into *E. coli* BL21(DE3) pLys Express cells (New England Biolabs). AlS was cultured in 2 × YT medium at 37 °C until an OD<sub>600</sub> ~ 1.3 was reached, and subsequently cooled to 18 °C. Protein expression was induced by addition of isopropyl-β-D-thiogalactopyranoside (IPTG, 0.5 mM). Cells were grown overnight and were harvested by centrifugation (9000 g, 10 min, 4 °C). The pellet was resuspended in Tris·HCl (50 mM pH 8.0) containing NaCl (500 mM) and MgCl<sub>2</sub> (1 mM). The cells were lysed by sonication at 4 °C, and the supernatant was cleared by centrifugation (48000 g, 1 h, 4 °C). Ni<sup>2+</sup>-NTA (~1 mL; GE Healthcare) was equilibrated with Tris·HCl (20 mM, pH 8.0) containing NaCl (500 mM), MgCl<sub>2</sub> (1 mM), imidazole (10 mM), and DTT (2 mM). AlS<sup>C-His</sup> was loaded on the column and washed with equilibration buffer (3 cv). AlS<sup>C-His</sup> was eluted in Tris·HCl (20 mM, pH 8.0) containing NaCl (500 mM), MgCl<sub>2</sub> (1 mM), DTT (2 mM), and imidazole (500 mM). The cleared AlS<sup>wt</sup> supernatant was diluted (1:10) with Tris·HCl (50 mM, pH 8.0) containing MgCl<sub>2</sub> (1 mM), and loaded on a 1 mL HiTrap Q XL column (GE Healthcare). AlS<sup>wt</sup> was eluted in a linear NaCl gradient (100–1000 mM). The pooled fractions were diluted (1:10) in Tris·HCl (50 mM, pH 8.0) with MgCl<sub>2</sub> (1 mM) and loaded on a MonoQ 10/100 column (GE Healthcare). AlS<sup>wt</sup> was eluted in a linear NaCl gradient (100–1000 mM). Size-exclusion chromatography of AlS<sup>wt</sup> and AlS<sup>C-His</sup> was performed with a HighLoad Superdex S200 16/60 column (GE Healthcare) equilibrated with Tris·HCl (50 mM, pH 8.0) containing NaCl (100 mM), MgCl<sub>2</sub> (1 mM), and DTT (2 mM). Pooled fractions were concentrated with Amicon-Ultra 30000 filters to 35 mg mL<sup>-1</sup> as determined by absorbance at 280 nm.

**Crystallization and crystal cooling:** For cofactor incorporation, AlS<sup>wt</sup> or AlS<sup>C-His</sup> (35 mg mL<sup>-1</sup>) was incubated (3.5 h, RT) with ThDP (1 mM) and Mg<sup>2+</sup> (2 mM), then used for crystallization experiments by the sitting drop method with a reservoir solution of polyethylene glycol 300 (30%, v/v), CaAc (200 mM), and sodium cacodylate (100 mM, pH 6.5). Crystals of AlS<sup>C-His</sup> appeared after one day. AlS<sup>wt</sup> was crystallized with PEG 200 (45%, v/v), Tris·HCl (100 mM, pH 7.0), and Li<sub>2</sub>SO<sub>4</sub> (50 mM). The crystals were flash cooled in liquid nitrogen without cryo-protectant. Soaking experiments were performed

with a reservoir solution supplemented with pyruvate (2 mM). After 3 s the crystals were flash frozen in liquid nitrogen.

**X-ray data collection, structure determination, and refinement:** Synchrotron diffraction data were collected at MX Beamline 14.2 at BESSY (Berlin, Germany) or Beamlines P13 and P14 of Petra III (Deutsches Elektronen Synchrotron, Hamburg, Germany). X-ray data collection was performed at 100 K. Diffraction data were processed with the XDS package (Table 1).<sup>[38,39]</sup> For calculation of the free R-factor, a randomly generated set of 5% of the reflections from the diffraction data set was used and excluded from the refinement. Initial phases of the AlS<sup>C-His</sup> were determined by molecular replacement with PHASER<sup>[40]</sup> and a search model of one monomer derived from the coordinates of AlS<sup>K</sup> (PDB ID: 1OZF)<sup>[19]</sup> that had been side-chain and cofactor depleted. An initial model was built with the program BUCCANEER.<sup>[41]</sup> The structure was initially refined by applying a simulated annealing protocol, and in subsequent refinement cycles maximum-likelihood restrained refinement in PHENIX<sup>[42]</sup> was used, followed by iterative, manual model building with COOT.<sup>[43]</sup> AlS<sup>wt</sup> diffraction data were analyzed with PHENIX.XTRIAGE.<sup>[44]</sup> The structure of AlS<sup>wt</sup> in the small unit cell was solved by molecular replacement with one protomer of the initially built AlS<sup>C-His</sup> with the program PHASER.<sup>[40]</sup> The structure of AlS<sup>wt</sup> was refined with PHENIX.REFINE.<sup>[42]</sup> Water molecules were located with COOT<sup>[43]</sup> and manually inspected. Model quality was evaluated with PROCHECK<sup>[45]</sup> and MolProbity.<sup>[46]</sup> Figures were prepared using PyMOL.<sup>[47]</sup> The active-site tunnel was calculated with the PyMOL plug-in CAVER.<sup>[48]</sup> The atomic coordinates and structure factor amplitudes have been deposited in the Protein Data Bank (IDs: 4RJ, 4RJJ, and 4RJK).

**Heterologous expression and enzyme purification for enzymatic assays:** AlS<sup>C-His</sup> and all AlS<sup>C-His</sup> variant expression was performed in *E. coli* HMS174(DE3) cells in TB medium supplemented with kanamycin (50 μg mL<sup>-1</sup>). After inoculation cells were grown to OD<sub>600</sub> = 0.5–0.7 at 37 °C and subsequently induced with IPTG (1 mM). The temperature was decreased to 16 °C for further culturing (48 h). Cell lysates were prepared with and Emulsiflex-B15 cell disruptor (Avestin, Mannheim, Germany), and cell debris was removed by centrifugation (25000 g, 20 min, 4 °C). Protein purification was performed with Ni<sup>2+</sup>-NTA. Desalting of the proteins was performed with PD-10 columns (GE Healthcare). All variants were purified as described for AlS<sup>C-His</sup>. AlS<sup>C-His</sup> and its variants were stored at –80 °C with the buffer supplemented with glycerol 10% (v/v). Protein concentration was measured at 280 nm with unfolded protein in 8 M urea.<sup>[49]</sup> The extinction coefficient was calculated using the ExPASy ProtParam tool.<sup>[50]</sup>

**Enzyme assays:** Pyruvate and KIV assays were performed by UV/Vis spectrophotometry in 96-well microtiter plates with an EnSpire 2 plate reader (PerkinElmer). The buffer pH was adjusted to the corresponding temperature according to Stoll and Blanchard.<sup>[51]</sup> One unit of enzyme activity is defined as the amount of enzyme necessary to convert 1 μmol substrate per minute. For the pyruvate assay, reaction mixtures in HEPES (50 mM, pH 7), ThDP (0.1 mM), MgCl<sub>2</sub> (10 mM), and sodium pyruvate (15 mM) were incubated at RT. The activity of AlS/variant was measured by assaying the pyruvate consumption at 50 °C (in a water bath), with standard LDH assay triplicates.<sup>[31]</sup> Samples (4 μL) of each assay were taken every five minutes. The remaining pyruvate in each sample was immediately converted to lactate by LDH. The aliquot (4 μL, = 0.3 mM sodium pyruvate in the control (without enzyme)) was transferred to the LDH assay mixture at RT (HEPES (25 mM, pH 7.4), NADH (0.3 mM), sodium pyruvate (0–0.3 mM)). NADH absorbance was determined at 340 nm. For thermal stability assays, AlS was stored



over several days at 50 °C in a water bath. For solvent stability assays, the previously standardized reaction mixture contained the tested amount of 1-butanol, ethanol, or isobutanol. All assays were performed at 50 °C. Determination of optimum pH was performed with either sodium acetate (pH 4.0–5.5), sodium phosphate (pH 6.0 and 6.5), Tris (pH 7.0–9.0), or CAPS (pH 10.0 and 11.0) at 50 °C. For the KIV assay, the reaction mixtures contained HEPES (50 mM, pH 7.0), ThDP (0.1 mM), MgCl<sub>2</sub> (2.5 mM), KIV (30 mM), NADH (0.3 mM), and ADH (0.25 U/mL). The activity of AlsS towards KIV was assayed at 40 °C with detection at 340 nm.

## Acknowledgements

We are grateful to Claudia Alings for excellent technical support. We thank Thomas Schneider for access and support at beamline P14 of PETRA III (Deutsches Elektronen Synchrotron, Hamburg, Germany). We accessed beamlines of the BESSY II (Berliner Elektronenspeicherring-Gesellschaft für Synchrotronstrahlung II) storage ring (Berlin, Germany) via the Joint Berlin MX-Laboratory sponsored by the Helmholtz Zentrum Berlin für Materialien und Energie, the Freie Universität Berlin, the Humboldt-Universität zu Berlin, the Max-Delbrück Centrum, and the Leibniz-Institut für Molekulare Pharmakologie.

**Keywords:** biofuels • biosynthesis • biotechnology • enzyme catalysis • isobutanol

- [1] S. Atsumi, T. Hanai, J. C. Liao, *Nature* **2008**, *451*, 86–89.
- [2] S. Atsumi, Z. Li, J. C. Liao, *Appl. Environ. Microbiol.* **2009**, *75*, 6306–6311.
- [3] S. Atsumi, T.-Y. Wu, E.-M. Eckl, S. D. Hawkins, T. Buelter, J. C. Liao, *Appl. Microbiol. Biotechnol.* **2010**, *85*, 651–657.
- [4] E. A. Savrasova, A. D. Kivero, R. S. Shakulov, N. V. Stoyanova, *J. Ind. Microbiol. Biotechnol.* **2011**, *38*, 1287–1294.
- [5] A. Baez, K.-M. Cho, J. C. Liao, *Appl. Microbiol. Biotechnol.* **2011**, *90*, 1681–1690.
- [6] J.-K. Guterl, D. Garbe, J. Carsten, F. Steffler, B. Sommer, S. Reiß, A. Philipp, M. Haack, B. Rühmann, A. Koltermann, U. Kettling, T. Brück, V. Sieber, *ChemSusChem* **2012**, *5*, 2165–2172.
- [7] A. F. Cann, J. C. Liao, *Appl. Microbiol. Biotechnol.* **2008**, *81*, 89–98.
- [8] C. R. Shen, J. C. Liao, *Metab. Eng.* **2008**, *10*, 312–320.
- [9] M. R. Connor, J. C. Liao, *Curr. Opin. Biotechnol.* **2009**, *20*, 307–315.
- [10] *GESTIS—Substance Database*, Sankt Augustin, (Germany), **2011**.
- [11] M. C. Renna, N. Najimudin, L. R. Winik, S. A. Zahler, *J. Bacteriol.* **1993**, *175*, 3863–3875.
- [12] O. Maestri, F. Joset, *Mol. Microbiol.* **2000**, *37*, 828–838.
- [13] S. Li, J. Wen, X. Jia, *Appl. Microbiol. Biotechnol.* **2011**, *91*, 577–589.
- [14] J. A. McCourt, R. G. Duggleby, *Amino Acids* **2006**, *31*, 173–210.
- [15] J. V. Schloss, D. E. Van Dyk, *Methods Enzymol.* **1988**, *166*, 445–454.
- [16] R. G. Duggleby, S. S. Pang, *J. Biochem. Mol. Biol.* **2000**, *33*, 1–36.
- [17] S. S. Pang, R. G. Duggleby, L. W. Guddat, *J. Mol. Biol.* **2002**, *317*, 249–262.
- [18] J.-G. Wang, P. K.-M. Lee, Y.-H. Dong, S. S. Pang, R. G. Duggleby, Z.-M. Li, L. W. Guddat, *FEBS J.* **2009**, *276*, 1282–1290.
- [19] S. S. Pang, R. G. Duggleby, R. L. Schowen, L. W. Guddat, *J. Biol. Chem.* **2004**, *279*, 2242–2253.
- [20] S. Zhang, M. Liu, Y. Yan, Z. Zhang, F. Jordan, *J. Biol. Chem.* **2004**, *279*, 54312–54318.
- [21] D. Meyer, P. Neumann, C. Parthier, R. Friedemann, N. Nemeria, F. Jordan, K. Tittmann, *Biochemistry* **2010**, *49*, 8197–8212.
- [22] F. H. Andrews, M. J. McLeish, *Bioorg. Chem.* **2012**, *43*, 26–36.
- [23] A. Schütz, R. Golbik, S. König, G. Hübner, K. Tittmann, *Biochemistry* **2005**, *44*, 6164–6179.
- [24] R. Kluger, K. Tittmann, *Chem. Rev.* **2008**, *108*, 1797–1833.
- [25] Y. A. Muller, G. E. Schulz, *Science* **1993**, *259*, 965–967.
- [26] J. M. Candy, R. G. Duggleby, *Biochim. Biophys. Acta Protein Struct. Mol. Enzymol.* **1998**, *1385*, 323–338.
- [27] Y. Lindqvist, G. Schneider, U. Ermler, M. Sundström, *EMBO J.* **1992**, *11*, 2373–2379.
- [28] R. Breslow, *J. Am. Chem. Soc.* **1957**, *79*, 1762–1763.
- [29] G. Wille, D. Meyer, A. Steinmetz, E. Hinze, R. Golbik, K. Tittmann, *Nat. Chem. Biol.* **2006**, *2*, 324–328.
- [30] K. Tittmann, R. Golbik, K. Uhlemann, L. Khailova, G. Schneider, M. Patel, F. Jordan, D. M. Chipman, R. G. Duggleby, G. Hübner, *Biochemistry* **2003**, *42*, 7885–7891.
- [31] S. Wolterink-van Loo, A. van Eerde, M. A. J. Siemerink, J. Akerboom, B. W. Dijkstra, J. van der Oost, *Biochem. J.* **2007**, *403*, 421–430.
- [32] S.-C. Lee, J. Kim, I.-J. La, S.-K. Kim, M.-Y. Yoon, *Enzyme Microb. Technol.* **2013**, *52*, 54–59.
- [33] V. Gedi, M.-Y. Yoon, *FEBS J.* **2012**, *279*, 946–963.
- [34] W. D. Holtzclaw, L. F. Chapman, *J. Bacteriol.* **1975**, *121*, 917–922.
- [35] C. L. Young, Z. T. Britton, A. S. Robinson, *Biotechnol. J.* **2012**, *7*, 620–634.
- [36] R. L. Schowen, *Thiamin-Dependent Enzymes*, Academic Press, London, **1998**.
- [37] S. Barik in *Methods in Molecular Biology*, Vol. 57: *Site-Directed Mutagenesis in Vitro by Megaprimer PCR* (Ed.: M. K. Trower), Humana, Totowa, **1996**, pp. 203–215.
- [38] W. Kabsch, *Acta Crystallogr. Sect. D Biol. Crystallogr.* **2010**, *66*, 125–132.
- [39] M. Krug, M. S. Weiss, U. Heinemann, U. Mueller, *J. Appl. Crystallogr.* **2012**, *45*, 568–572.
- [40] A. J. McCoy, R. W. Grosse-Kunstleve, P. D. Adams, M. D. Winn, L. C. Storoni, R. J. Read, *J. Appl. Crystallogr.* **2007**, *40*, 658–674.
- [41] K. Cowtan, *Acta Crystallogr. Sect. D Biol. Crystallogr.* **2008**, *64*, 83–89.
- [42] P. V. Afonine, R. W. Grosse-Kunstleve, N. Echols, J. J. Headd, N. W. Moriarty, M. Mustyakimov, T. C. Terwilliger, A. Urzhumtsev, P. H. Zwart, P. D. Adams, *Acta Crystallogr. Sect. D Biol. Crystallogr.* **2012**, *68*, 352–367.
- [43] P. Emsley, B. Lohkamp, W. G. Scott, K. Cowtan, *Acta Crystallogr. Sect. D Biol. Crystallogr.* **2010**, *66*, 486–501.
- [44] P. D. Adams, P. V. Afonine, G. Bunkóczi, V. B. Chen, I. W. Davis, N. Echols, J. J. Headd, L.-W. Hung, G. J. Kapral, R. W. Grosse-Kunstleve, A. J. McCoy, N. W. Moriarty, R. Oeffner, R. J. Read, D. C. Richardson, J. S. Richardson, T. C. Terwilliger, P. H. Zwart, *Acta Crystallogr. Sect. D Biol. Crystallogr.* **2010**, *66*, 213–221.
- [45] R. A. Laskowski, M. W. McArthur, D. S. Moss, J. M. Thornton, *J. Appl. Crystallogr.* **1993**, *26*, 283–291.
- [46] V. B. Chen, W. B. Arendall III, J. J. Headd, D. A. Keedy, R. M. Immormino, G. J. Kapral, L. W. Murray, J. S. Richardson, D. C. Richardson, *Acta Crystallogr. Sect. D Biol. Crystallogr.* **2010**, *66*, 12–21.
- [47] <http://www.pymol.org>.
- [48] E. Chovancova, A. Pavelka, P. Benes, O. Strnad, J. Brezovsky, B. Kozlikova, A. Gora, V. Sustr, M. Klvana, P. Medek, L. Biedermannova, J. Sochor, J. Damborsky, *PLoS Comput. Biol.* **2012**, *8*, e1002708.
- [49] C. N. Pace, F. Vajdos, L. Fee, G. Grimsley, T. Gray, *Protein Sci.* **1995**, *4*, 2411–2423.
- [50] “Protein Identification and Analysis Tools on the ExPASy Server”, E. Gasteiger, C. Hoogland, A. Gattiker, S. Duvaud, M. R. Wilkins, R. D. Appel, A. Bairoch in *The Proteomics Protocols Handbook* (Ed.: J. M. Walker), Humana, Totowa, **2005**, pp. 571–607.
- [51] V. S. Stoll, J. S. Blanchard, *Methods Enzymol.* **2009**, *463*, 43–56.

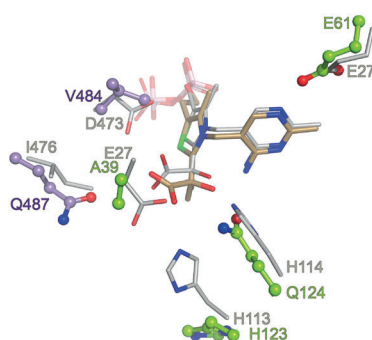
Received: September 17, 2014  
Published online on ■■■■■, 0000

## FULL PAPERS

B. Sommer, H. von Moeller, M. Haack,  
F. Qoura, C. Langner, G. Bourenkov,  
D. Garbe, B. Loll,\* T. Brück\*



**Detailed Structure–Function  
Correlations of *Bacillus subtilis*  
Acetolactate Synthase**



**Acetolactate synthase (ALS)** is an essential enzyme in designed isobutanol biosynthesis pathways. Because of its efficient catalytic conversion of pyruvate to acetolactate and its reactivity towards the alternative substrate ketoisovalerate (KIV), the ALS of *B. subtilis* is of particular interest. This study provides new insights into the structure–function relationships of this catalytic mechanism.